Mon. Not. R. Astron. Soc. **000**, 000–000 (0000) Printed 19 February 2014 (MN LATEX style file v2.2)

Low redshift quasars in the SDSS Stripe 82. The host galaxies.

R. Falomo[1⋆], D. Bettoni[1], K. Karhunen[2], J. K. Kotilainen[3], and M. Uslenghi[4]
[1] *INAF – Osservatorio Astronomico di Padova, Vicolo dell'Osservatorio 5, I-35122 Padova (PD), Italy*
[3] *Finnish Centre for Astronomy with ESO (FINCA), University of Turku, Väisäläntie 20, FI-21500 Piikkiö, Finland*
[2] *Tuorla Observatory, Department of Physics and Astronomy, University of Turku, FI-21500 Piikkio, Finland.*
[4] *INAF-IASF via E. Bassini 15, 20133 - Milano, Italy*

arXiv:1402.4300v1 [astro-ph.GA] 18 Feb 2014

19 February 2014

ABSTRACT

We present a photometrical and morphological study of the properties of low redshift (z < 0.5) quasars based on a large and homogeneous dataset of objects derived from the Sloan Digital Sky Survey (DR7). This study over number by a factor ∼ 5 any other previous study of QSO host galaxies at low redshift undertaken either on ground or on space surveys. We used ∼ 400 quasars that were imaged in the SDSS Stripe82 that is up to 2 mag deeper than standard Sloan images. For these quasars we undertake a study of the host galaxies and of their environments. In this paper we report the results for the quasar hosts.

We are able to detect the host galaxy for more than 3/4 of the whole dataset and characterise the properties of their hosts. We found that QSO hosts are dominated by luminous galaxies of absolute magnitude M*-3 < M(R) < M*. For the unresolved objects we computed a upper limit to the host luminosity. For each well resolved quasar we are also able to characterise the morphology of the host galaxy that turn out to be more complex than what found in previous studies. QSO are hosted in a variety of galaxies from pure ellipticals to complex/composite morphologies that combine spheroids, disk, lens and halo.

The black hole mass of the quasar, estimated from the spectral properties of the nuclei, are poorly correlated with the total luminosity of the host galaxy. However, taking into account only the bulge component we found a significant correlation between the BH mass and the bulge luminosity of the host.

1 INTRODUCTION

Accretion onto a supermassive black hole (SMBH) is the main mechanism that sustains the powerful activity of active galactic nuclei but may also represent a common phase in the evolution of normal galaxies. A number of fundamental question about the formation of the QSO phenomenon like the fuelling and triggering mechanisms are strictly related to the immediate environments of the active nucleus and in particular to its host galaxy (Merloni et al. 2010). SMBHs may well have a period of maximum growth (maximum nuclear luminosity) contemporaneous with the bulk of the initial star formation in the bulge of galaxies. Studies of the co-evolution of SMBH and their host spheroids are therefore obviously critical to understanding how and when galaxies in the local Universe formed and evolved. The last ten years have yielded considerable progress in characterising AGN host galaxies. At variance with inactive galaxies their study is often hampered by the presence of the luminous central source that outshines the light of the host galaxy. A problem that becomes more serious for high luminosity AGNs and for sources at high redshift.

In spite of these limitations the characterization of the properties of the host galaxies offers the unique opportunity to investigate the link between the central black hole mass and its host galaxy at moderate to high redshift and to trace the possible co-evolution at different cosmic epochs. This is because for broad line AGN like quasars it is possible to estimate the mass of the central BH using kinematic arguments that are not directly dependent on the host galaxies properties.

Both ground-based and HST studies have shown that virtually all luminous low redshift (z<0.5) quasars reside in massive, spheroid-dominated host galaxies, whereas at lower luminosities quasars can also be found in early- type spiral hosts (e.g. Bahcall et al. 1997; Dunlop et al. 2003; Pagani et al. 2003; Floyd et al. 2004; Jahnke et al. 2004). This is in good agreement with the BH – bulge relationship in inactive galaxies (e.g. Gultekin et al. 2009), since very massive BHs power luminous quasars. Only a small fraction of the host galaxies (∼15%) are found in merger systems but it is difficult to determine clear merger signatures from morphology alone. At low redshifts a major contribution to the properties of quasar host galaxies has been provided by

© 0000 RAS

images from the Hubble Space Telescope (HST). The improved spatial resolution has allowed the characterization of the structure and the detailed morphology of the host galaxies (Bahcall et al. 1997; Kukula et al. 2001; Ridgway et al. 2001; Dunlop et al. 2003; Peng et al. 2006; Zakamska et al. 2006). It turned out that QSO are hosted in luminous galaxies that are often dominated by the spheroidal component.

At high redshift (z >1) HST observations of quasar host galaxies (e.g. Peng et al. (2006); Floyd et al. (2013) and references therein) have been complemented by significant contributions from 8-m class ground-based telescopes under superb seeing conditions (Kotilainen et al. 2007, 2009) and/or with adaptive optics (Falomo et al. 2008). Comparison of host galaxies of AGN at high and low redshift constrain host galaxy evolution, as compared with the evolution of normal (inactive) galaxies.

Most of the old studies of quasar host considered few tens of objects therefore in order to derive a picture of the host properties at various redshift one should combine many different samples often obtained with different telescopes and filters. Observations carried out by HST are certainly more homogeneous (although different filters were used) and allow to investigate a somewhat large sample based on high quality data. Nevertheless the size of these samples remain relatively small For instance in the range $0.25 < z < 0.5$ about 50 QSO were imaged by HST (see references above).

In order to explore a significantly larger dataset of QSO one should refer to large surveys that include both imaging and spectroscopic data. In this respect one of the most productive recent surveys is the Sloan Digital Sky Survey that allowed to find 105783 quasars (Schneider et al. 2010) from (DR-7). Standard SDSS images are, however, too shallow and the faint nebulosity around the nucleus of quasars is not detected. This problem has been overcome in the case of the special sky region mapped by SDSS for the SDSS Legacy Survey.

The central stripe in the South Galactic Gap, namely the Stripe82 (Annis et al. 2011) is a stripe along the Celestial Equator in the Southern Galactic Cap. It is $2.5^{\rm deg}$ wide and covers -$50^{\rm deg}$ $\leqslant$RA$\leqslant$+ $60^{\rm deg}$, so its total area is 275deg^2. Stripe 82 was imaged by the SDSS multiple times, these data were taken in 2004 only under optimal seeing, sky brightness, and photometric conditions (i.e., the conditions required for imaging in the main Legacy Survey; York et al. (2000)). In 2005-2007, 219 additional imaging runs were taken on Stripe 82 as part of the SDSS supernova survey (Frieman et al. 2008), designed to discover Type Ia supernovae at $0.1< z <0.4$. The total number of images reaches $\sim$100 for the S strip and $\sim$ 80 for the N strip. The final frames were obtained by co-adding selected fields in r-band, with seeing (as derived from 2D gaussian fit of stars and provided by SDSS pipeline) better than 2", sky brightness $\leqslant$19.5 $mag/arcsec^2$ and less than 0.2 mag of extinction. In this area there are 12434 quasars.

Recently Matsuoka et al. (2014) analyzed the stellar properties of about 800 galaxies hosting optically luminous, unobscured quasars at z< 0.6 using Stripe82 images. They focused on the color of the host galaxies and found that the quasar hosts are very blue and almost absent on the red sequence with a marked different distribution from that of normal (inactive) galaxies.

For our study we selected QSO with redshift less than 0.5 for which the stripe 82 images allow us also to study the QSO galaxy environments. We adopt the concordance cosmology with $H_0 = 70$ km s^{-1} Mpc^{-1}, $\Omega_m = 0.3$ and $\Omega_\Lambda = 0.7$.

In this first paper of a series we focus on the properties of quasar hosts and their relationship with the central BH mass in the explored redshift range. In forthcoming papers we investigate the galaxy environments (Karhunen et al. 2013) and galaxy peculiarities (Bettoni et al. 2014). A preliminary account of these results was presented in Kotilainen et al. (2013).

2 THE LOW Z QSO SAMPLE

To derive the sample of low redshift quasars we used the fifth release of the SDSS Quasar Catalog (Schneider et al. 2010) that is based on the SDSS-DR7 data release (Abazajian et al. 2009). It consists of QSO that have a highly reliable redshift measurement and are fainter than $i \sim 15.0$, that have an absolute magnitude M_i <-22, at least one emission line with FWHM>1000 km/ sec, or have complex/ interesting absorption lines. This catalog contain $\sim$106.000 spectroscopically confirmed quasars. Our analysis is done only in the region of sky covered by the stripe82 data, these images go deeper of about $\sim$2 magnitudes with respect to the usual Sloan data and make possible the study of the QSO hosts (see example in Fig. 1).

We apply two main constraints on the sample. First, we avoid objects that are closer than 0.2 deg to the edges of the Stripe82 (Annis et al. 2011; Abazajian et al. 2009). Second, we choose an upper redshift limit z=0.5 in order to be able to resolve the quasar host for the large majority of the sample.

To satisfy all these reasons we therefore select all the QSOs in the range of redshift $0.1 < z < 0.5$ and in the Stripe82 region i.e. $1.0 < DEC < -1.0$, $0 < RA < 59.8$ and $300.2 < RA < 360$. This gives a total of 416 QSOs. In this sample we are dominated by radio quiet quasars only 24 are radio loud (about 5%). In Fig. 2 we report the distribution of QSO in the plane z-M_i . The mean redshift of the sample is $< z > = 0.39 \pm 0.08$ (median 0.41 ± 0.06) and the average absolute magnitude is : $< M_i > = -22.68 \pm 0.61$ (median -22.52 ± 0.35).

In Table 1 we report the main data for the QSO in the sample. In column (1) id number, in column (2) the SDSS identification in columns (3) and (4) the coordinates, in column (5) the redshift, in column (6) the i band psf magnitude from SDSS-DR7, in column (7) the absolute i band magnitude, in column (8) the number of exposures for each co added frame, in column (9) the i band extinction and finally in column (10) the measured seeing on the co-added images. The images used have an average seeing, as given by 2D gaussian fit of stars in the frame from SDSS, of 1.20$\pm$0.09 arcsec, with a minimum of 1.01 and a maximum of 1.47 arcsec.

3 IMAGE ANALYSIS

We have retrieved all images of the selected QSO from SDSS Stripe 82 dataset (Annis et al. 2011) in the i band. This cor-

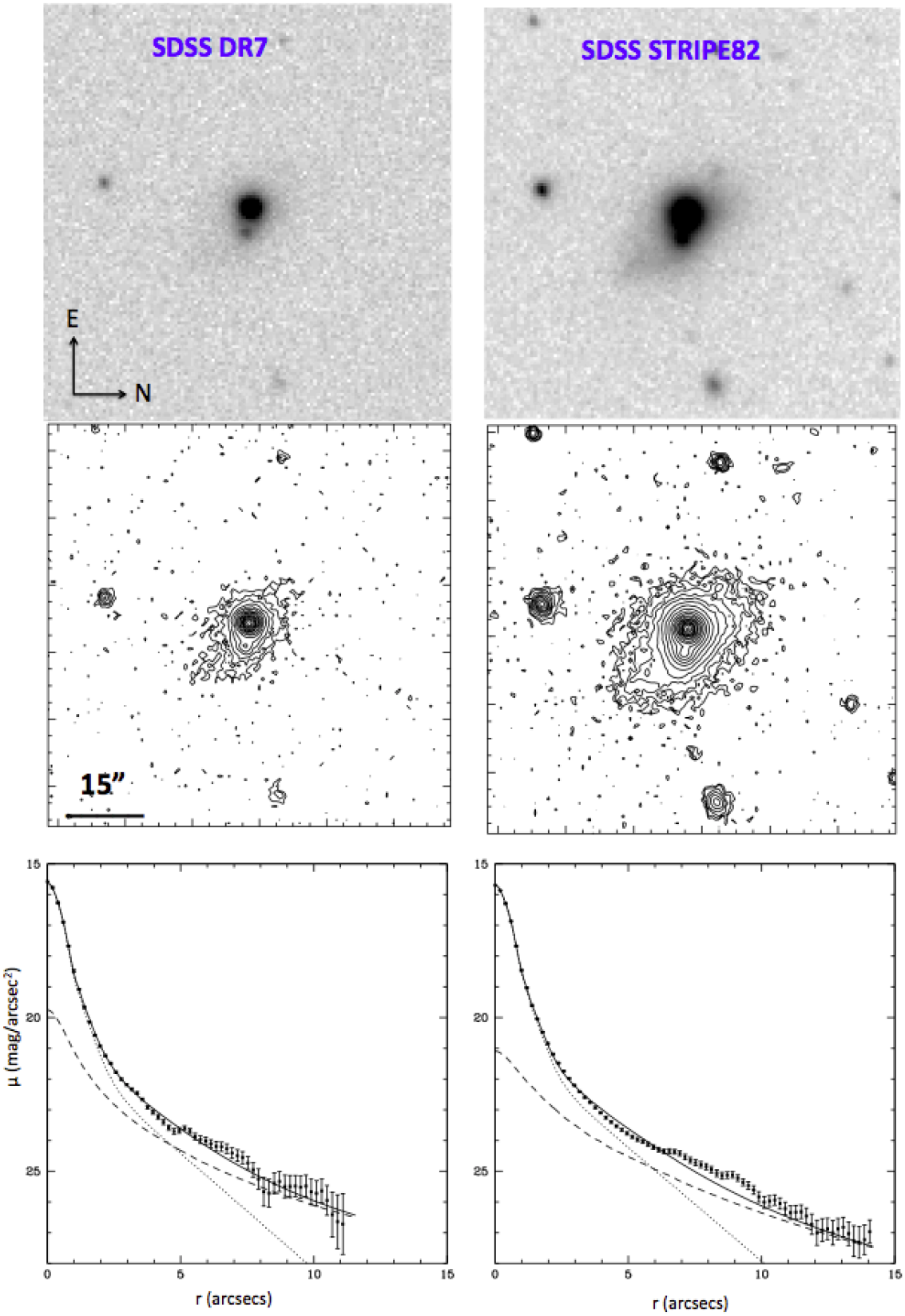

Figure 1. Example of QSO in the sample: Left panels show the SDSS DR7 data; Right panels the corresponding data from Stripe 82 (image resulting combining 35 individual images of 54 sec). Top panels yield the grey scale images in the i band; central panels give contour plots of the region and in the bottom panels we show the luminosity radial profiles together with the AIDA fit (see text for details)

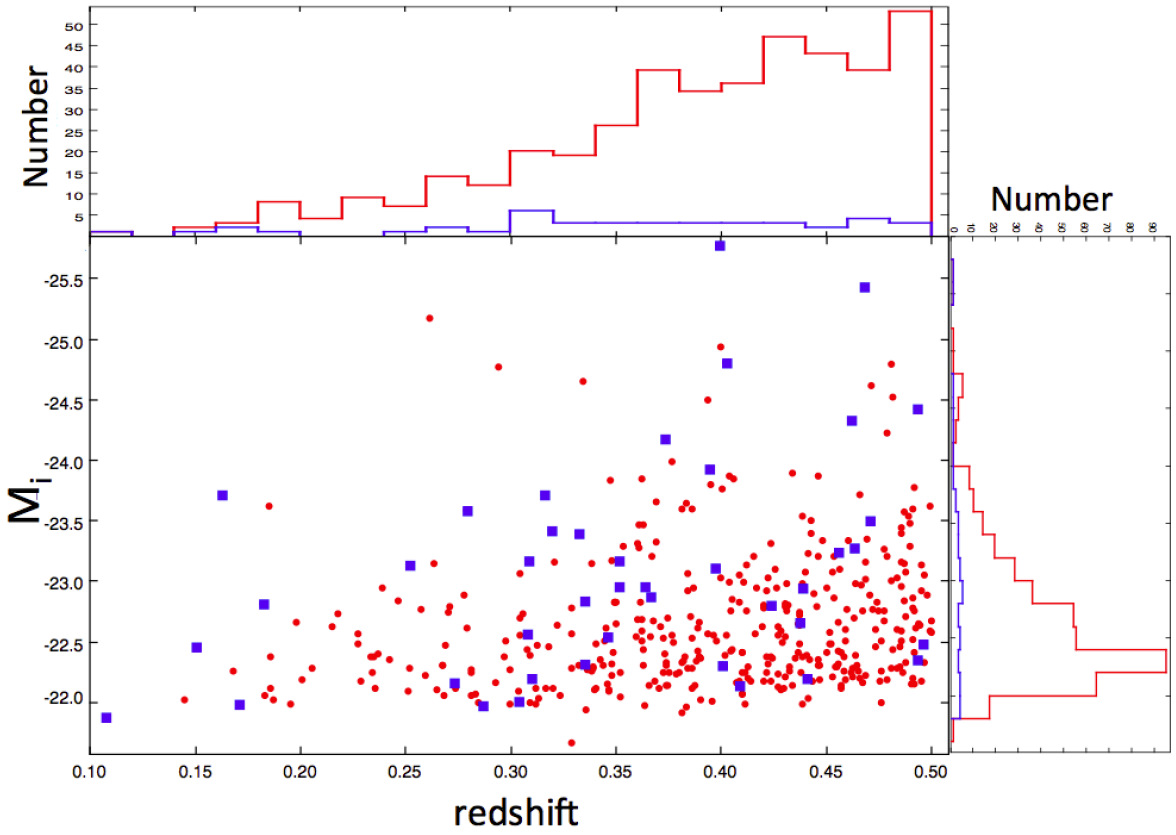

Figure 2. The QSO sample in the M_i redshift plane. Red filled circles are radio quiet while blue filled squares are radio loud QSOs. Top and right panels show the distributions of the redshift and luminosity for radio quiet (red) and radio loud (blue) objects.

responds to observe in the R filter at rest frame at the average redshift of the dataset. In order to derive the properties of the galaxies hosting the QSO we performed a 2D fit of the image of the QSO assuming it is the superposition of two components. The nucleus in the center and the surrounding nebulosity. The first is described by the local Point Spread Function of the image while for the second component we assumed a galaxy model described by a Sersic law convolved with the proper PSF. The analysis of these images was performed using the Astronomical Image Decomposition Analysis (AIDA, Uslenghi & Falomo (2008)) that was used in our previous studies of QSO host galaxies (Falomo et al. 2008; Decarli et al. 2012; Kotilainen et al. 2007, 2009).

The most critical aspect of the image decomposition is the determination of a suitable PSF. In the case of SDSS images the field of view is large enough that there are always many stars in the co-added SDSS image containing the target to properly derive the PSF. To derive the most suitable PSF of each field we have selected a number of stars (between 5 and 15) in the field that are distributed around the target. Selection of these PSF stars was based on various parameters as their magnitude, FWHM, ellipticity and presence of close companions. In particular, the selection of the stars was done according to the following criteria: the stars are not saturated; the stars are as close to the target as possible (while avoiding the fit region of the target); the stars are as uniformly distributed around the target as possible; the stars are sufficiently isolated (i.e., they have no close companions); the stars cover a suitably wide range of magnitude in order to assure that the extended halo of the PSF is well characterised.

We then define a radius to compute the PSF model and a ring around each star where to compute the sky background. All extra sources that were found inside these areas were masked out with an automated procedure. The PSF model was then obtained from the simultaneous fit of all selected stars using a multi function 2D model composed by 3 gaussians and one exponential function.

In Figure 3 we show an example of the procedure adopted to derive the PSF model. It is worth to note that the PSF provided by the SDSS pipeline (using source psField) are not adequate for this study. This is due to a systematic underestimate of the wings of the SDSS PSF. The agreement with our PSF model is excellent up to ~ 3 arcsec from the center of the star but then a significant deviation is present (see Figure 4). Using the SDSS psf for the QSO decomposition will result in a systematic overestimate of the host galaxy luminosity and in some cases to false detection of the host galaxy signal (see example in Figure 4 panel c))

The second step of the analysis is to fit each quasar both with a scaled PSF and with a 2 components model (point source plus a galaxy). The best fit was obtained adopting a model for the errors that include a constant term to represent the read out noise of the detector, a term representing the statistical noise due to the effective counts and an ad-

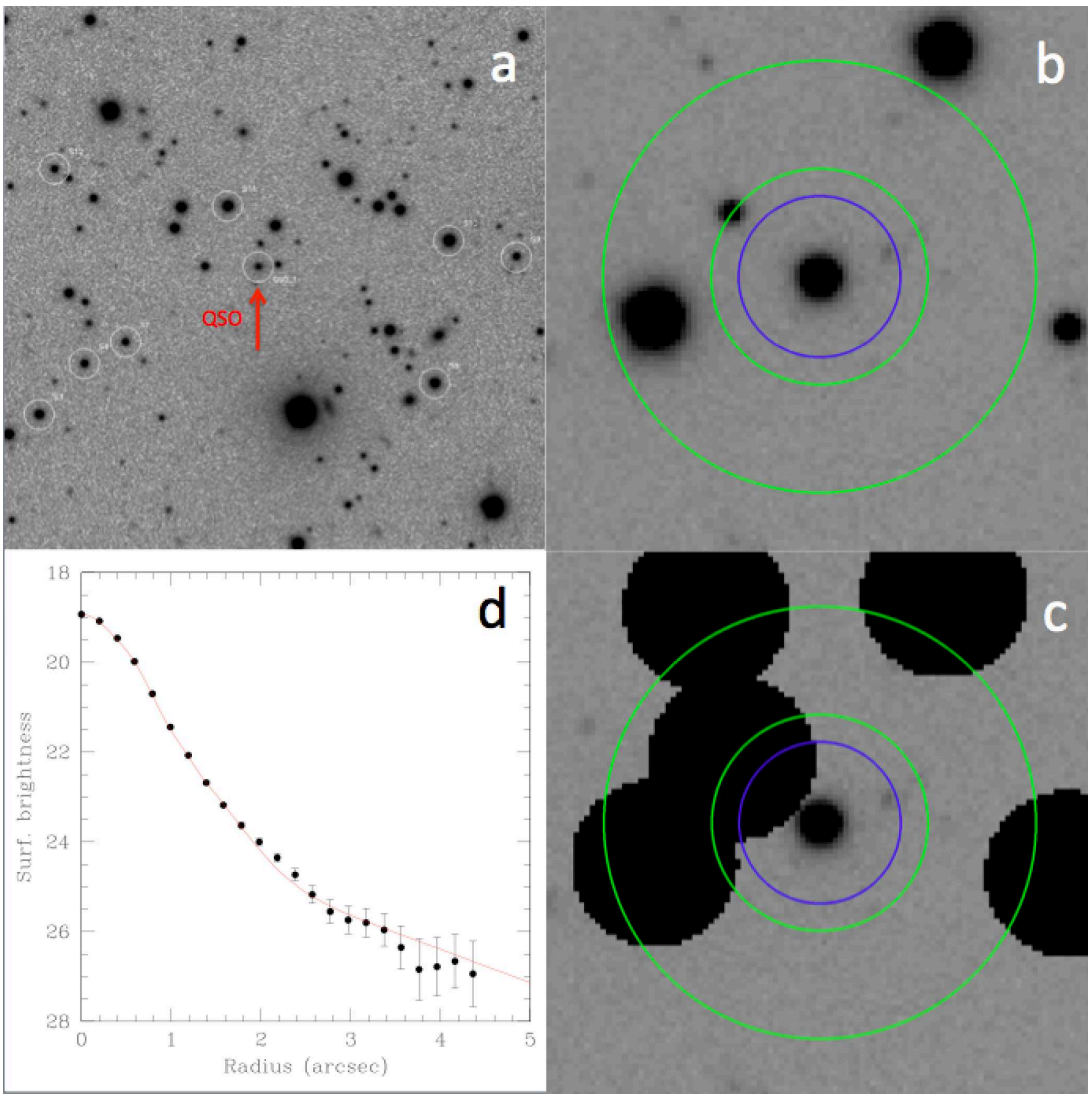

Figure 3. Modelling of the PSF: a) Selection of stars around the target; b) example of definition of fit area (inner blue circle) and the background region (encompassed by the two green circles) around one selected star; c) masked areas to avoid spurious sources; d) example of the model fit to the radial brightness profile of one selected star.

ditional term that take into account the possible residual noise due to fixed pattern noise. For the coadded images we assume a readout noise of 9.5 e^- and an average gain of 3.8 e^-/ADU. The term for the statistical noise is given by the coefficient $1/\sqrt{GAIN \times NEXP}$ that multiply the root square of the counts. For the residual pattern noise we assumed 2% value.

In Figure 5 we show an example of the adopted procedure. In order to distinguish between resolved and unresolved objects we compared the χ^2 of the two fits and in addition we then inspect all the fits to further check the results. This allows us to produce a clean list of $\sim$ 350 resolved quasars by removing 7 objects ($\sim$1% of the entire sample) that were contaminated by very bright sources in the field or defects in the image close to the targets. For 60 objects ($\sim$13% of the entire sample) the QSO were unresolved and the fit with only the psf was indistinguishable from the fit with the psf + Sersic function (see Figure 6). The unresolved objects are mainly objects at relatively high redshift (42 out of 60 unresolved quasars are at z $>$ 0.4) and bright nuclei.

For the unresolved objects we evaluated the bright limit of the host galaxy by adding the flux of a galaxy to the observed object until the χ^2 of fit to these data become 20% worst of that obtained from the fit with the scaled PSF. Since we have no knowledge of the underlying host galaxy we performed this evaluation of the brightness limit of the host galaxy using different models. We assumed two type of morphology : exponential disk and de Vaucoulers laws. Then we assume two values for the half light radius: 5 and 10 kpc that are representative values of the resolved objects in our sample The input half light radius in arcsec was derived assuming the redshift of the QSO. We took as upper limit to the luminosity of the host galaxy the maximum value derived from the various fit using different models and half light radius.

The final classification of the targets was based on the comparison of χ^2 for the two fit (only psf and psf + galaxy)

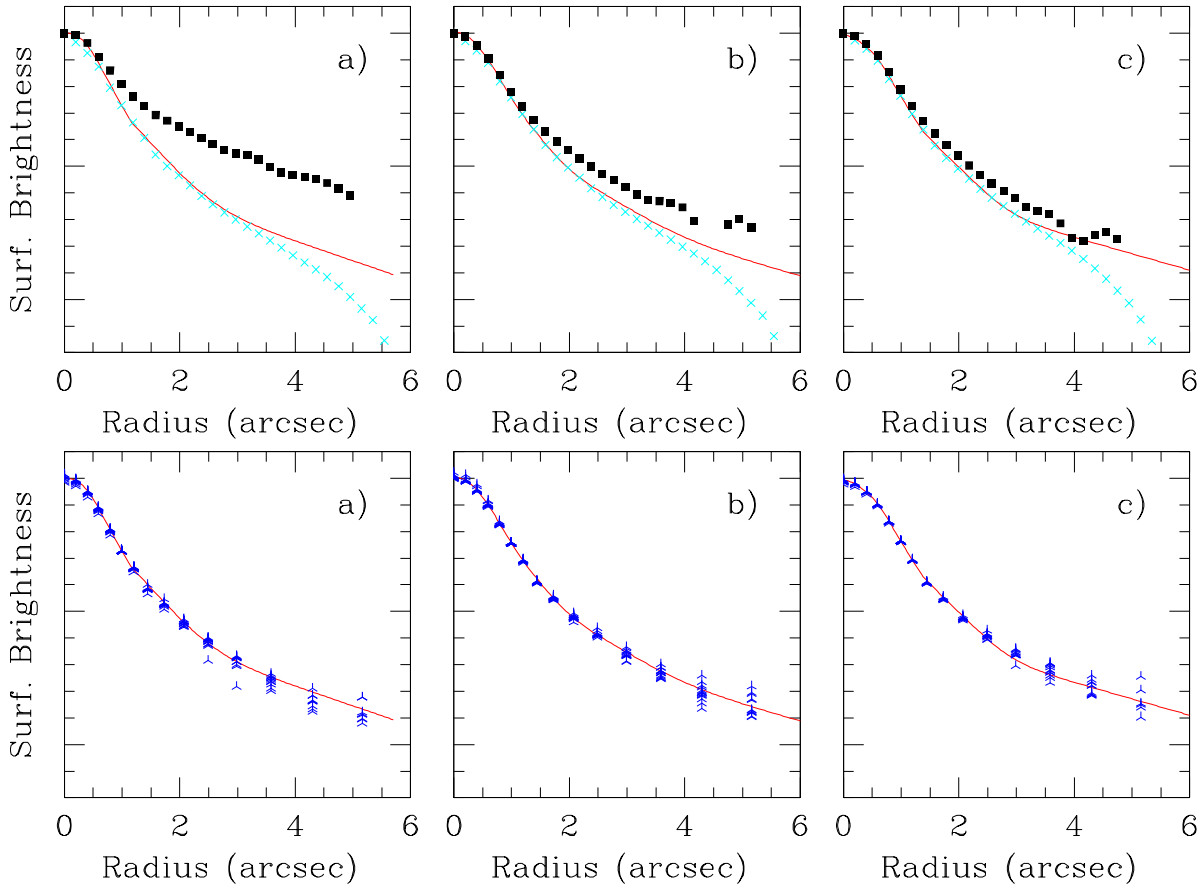

Figure 4. *Top panels*: Example of comparison between our PSF model (solid red line) and the PSF derived from SDSS archive (psField; light blue crosses) with the average radial brightness profile of three QSO (black filled squares). There is an excellent agreement for the two PSF until $\sim$ 3 arcsec from the center but beyond this radius the SDSS PSF systematically underestimate the flux from the wing of the psf. Panels a) (seeing = 1.1 arcsec) and b) (seeing = 1.22) show the average radial brightness distribution of well and marginally resolved objects, respectively, while the one in panel c) is unresolved. *Bottom panels*: Example of comparison between the average radial brightness profile of the adopted PSF model (solid red line) and that of the stars used to derive the PSF (blue points).

and further visual inspection of the fit. From this procedure we classified all objects as resolved, unresolved and marginally resolved for intermediate fit (see Figure 6 and Table 2).

4 HOST GALAXY PROPERTIES

In Figure 7 we show the distribution of the absolute magnitude of host galaxies for all (309) resolved quasars. These values were corrected for the galactic extinction (based on the values of SDSS) and k-corrected to the R band rest frame.

To perform the color and k-correction transformations, we assumed an elliptical and early type spiral galaxy spectral energy distribution (SED) template (Mannucci et al. (2001)) for the host galaxy. Because of the small difference of the templates in the observed spectral region, the k-correction adopting the two SEDs differ by few percent, thus we used for all objects the one for elliptical SED. For the nucleus we used a composite quasar spectrum (Francis et al. 1991). All k-corrections were performed adopting these templates for the SED and convolving them with the i and R filter responses. An example of the procedure is illustrated in Figure 8

The average absolute magnitude is $< M(R) >$ = -22.83 $\pm$ 0.6 (median -22.86 $\pm$ 0.36) . For comparison the distribution of absolute magnitude for a smaller ($\sim$ 100) sample of QSO observed by HST (see compilation by Decarli et al. (2010b)) in the similar redshift range is $< M(R) >$ = -23.00 $\pm$ 1.05. The two data sets are in excellent agreement in spite of the differences of observation technique. Five quasars in our sample were observed with Hubble Space Telescope and WFPC2 in filter F606W Cales et al. (2011) and it is possible to compare our analysis with the results from HST images. The comparison of the magnitudes of these host galaxies (assuming a color correction V-R = 0.8) is very good ($< \Delta m >$ = 0.1 $\pm$ 0.24)

The distribution of host galaxies in the redshift-luminosity plane (see Fig 9) confirms previous claims that they are encompassed between M* (M*(R) = –21.2 ; Nakamura et al. (2003)) and M* - 3 with more frequent distribution in the range M*-1 and M*-2 (Kukula et al. 2001; Dunlop et al. 2003; Falomo et al. 2004; Peng et al. 2006; Kotilainen et al. 2007; Decarli et al. 2010b).

There is a small, but significant, increasing of the host

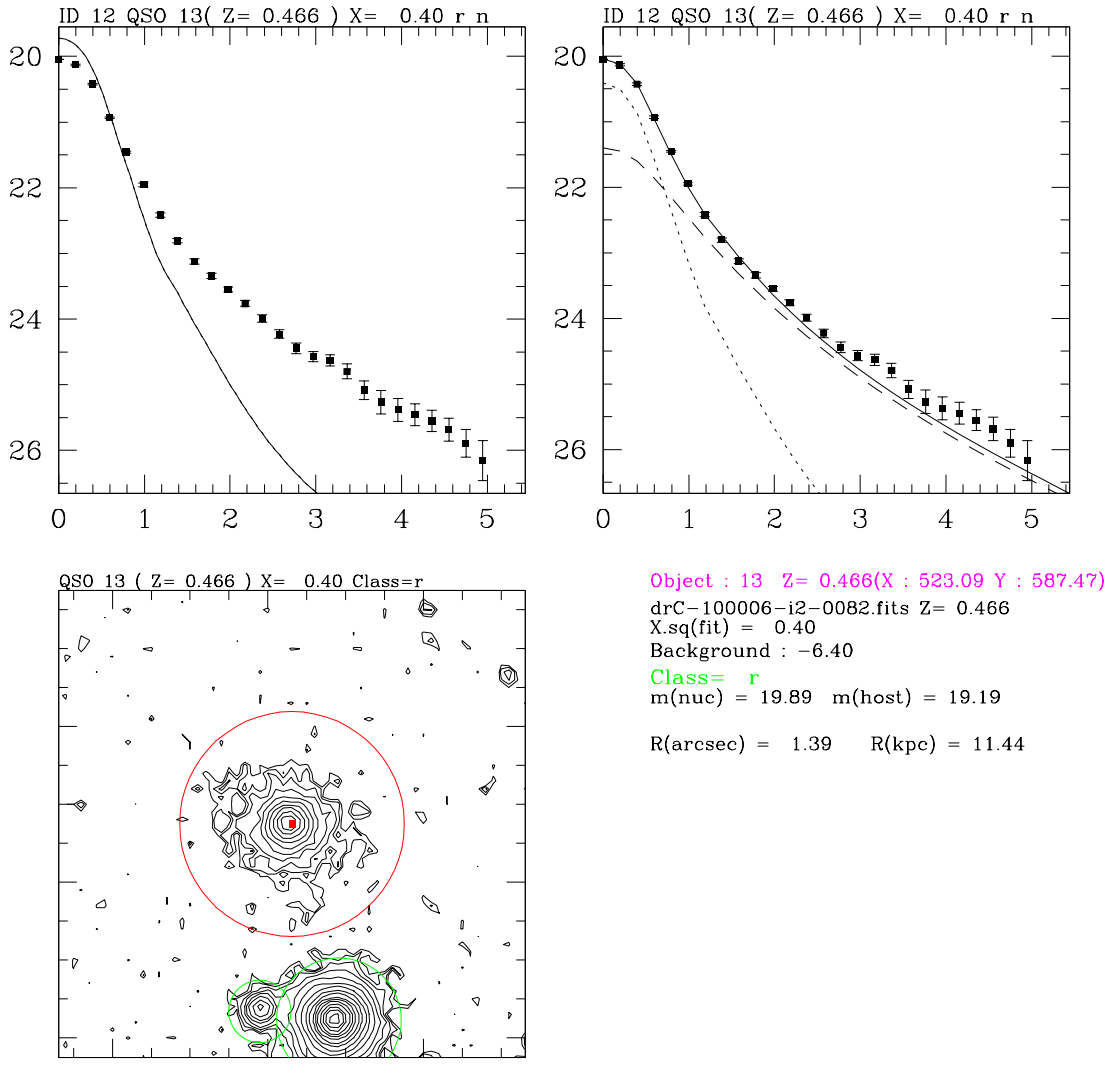
ID 12 QSO 13(Z= 0.466) X= 0.40 r n
ID 12 QSO 13(Z= 0.466) X= 0.40 r n
QSO 13 (Z= 0.466) X= 0.40 Class=r
Object : 13 Z= 0.466(X : 523.09 Y : 587.47)
drC-100006-i2-0082.fits Z= 0.466
X.sq(fit) = 0.40
Background : -6.40
Class= r
m(nuc) = 19.89 m(host) = 19.19
R(arcsec) = 1.39 R(kpc) = 11.44

Figure 5. Example of AIDA results for a resolved QSO. Bottom-left panel shows the contour plot of the target, the area of the fit (red circle) and the masked out objects in the field (green circles). Top-left panel shows the average radial brightness profile of the target and the best fit by a PSF model. Top-right panel: same as left panel but for the best fit of the target by nucleus (PSF) and host galaxy (Sersic law model). Solid line (best fit); dotted line PSF model; dashed line galaxy model convolved with psf

.

luminosity with the redshift (from M(R) $\sim$ -22.5 at z $\sim$0.2 to M(R) $\sim$ -23.1 at z $\sim$ 0.5) that is consistent with passive evolution of the underlying stellar population. A similar trend was also reported over a wider redshift range by Kotilainen et al. (2009).

While the total flux from the host galaxy is relatively well determined from the fit of resolved objects the evaluation of the half light radius is not well constrained. This is due to some degeneracy between the effective surface brightness and effective radius that can be combined to produce the same total flux. In Figure 10 we show the distribution of the effective radius (Re) as derived from the fit to the objects with a galaxy (modelled by a Sersic law) plus the nuclear component (modelled by PSF). The average effective radius is $< Re > = 7.7 \pm 3.6$ kpc. If we include only the targets with *good* fit (χ^2 / χ^2(PSF) $<$ 0.5) and uncertainty of Re $<$ 30% the average effective radius is slightly larger : $< Re > = 8.2 \pm 3.7$ kpc. For the small sample of radio loud quasars (17 objects) the average effective radius ($< Re > = 8.8 \pm 5.3$ kpc) is indistinguishable from that of the whole sample. In a hierarchical scenario of galaxy formation where one would expect that

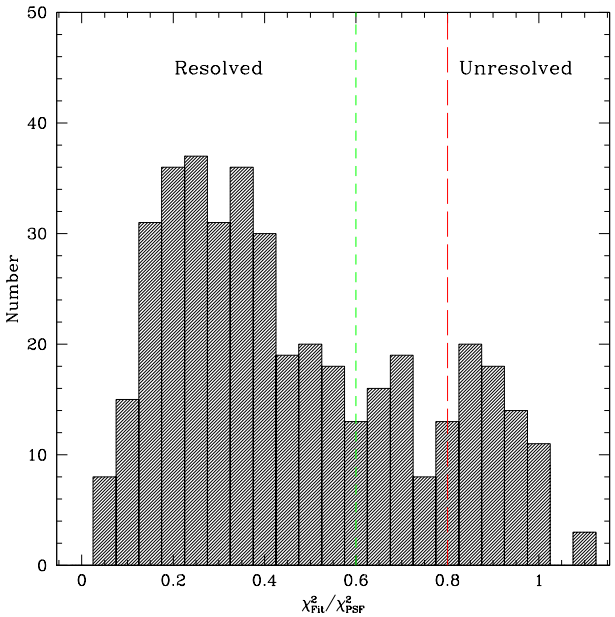

Figure 6. Distribution of the χ^2 ratio of the fit (PSF+galaxy) with respect to the one with only the PSF). The two vertical lines define the regions of our classification for objects resolved ($\chi^2_{Fit}/\chi^2_{PSF} < 0.6$), marginally resolved and unresolved ($\chi^2_{Fit}/\chi^2_{PSF} > 0.8$).

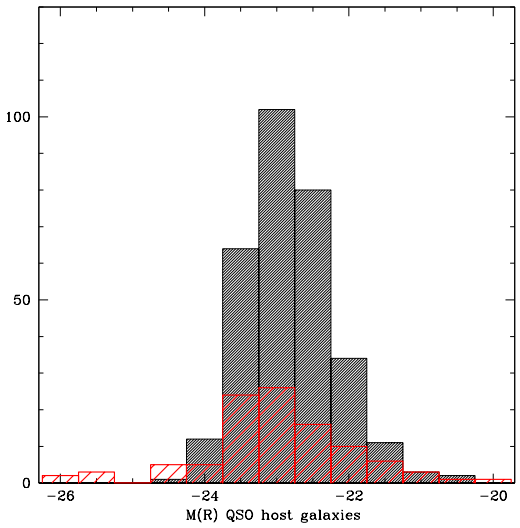

Figure 7. Absolute magnitude distribution of resolved QSO host galaxies in the rest frame R band. For comparison the distribution for a compilation of low redshift QSO imaged by HST is plotted (dashed red region) (Decarli et al. 2010b).

the size of galaxies evolve with the cosmic time as was reported in a number of detailed observations of galaxies at different redshift (e.g. Bouwens & Silk (2002); Bouwens et al. (2004); Trujillo et al. (2006); Ono et al. (2012)) the size of the galaxies (as derived from the half light radius) ranges from compact (few kpc) objects up to extended galaxies

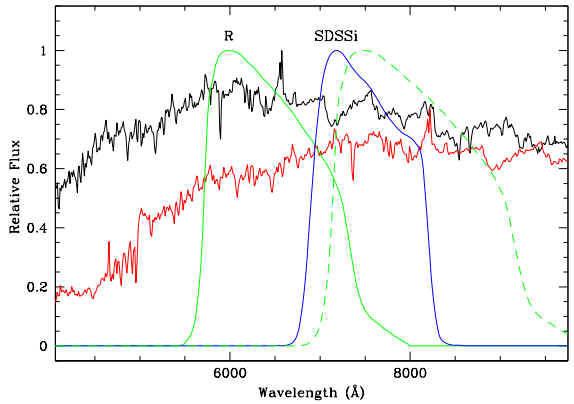

Figure 8. Example of k-correction and filter transformation for an object at z = 0.25 assuming a SED of an elliptical galaxy. The template for the elliptical galaxy is shown at rest frame (black line) and at z=0.25 (red line). The transmission for passbands R (solid green line) and i (blue line) are compared with the redshifted (z=0.25) R passband (dashed green line).

(10-15 kpc); in the observed redshift range we do not find any significant trend of change of the galaxy size with z. In some cases we found a significantly larger than average galaxy radius (see Fig. 10) that is likely due to the presence of an extended halo. These, and other peculiarities will be investigated in Bettoni et al. (2014).

An interesting controversial issue in the study of QSO and galaxies is the relationship between the nucleus and host galaxy luminosity. Assuming that quasars emit in a relatively narrow range of Eddington ratio and that the BH mass is correlated with the mass of the galaxy one would expect to find a correlation between nucleus and host galaxy luminosity. In figure 11 we show the comparison between the absolute magnitude of the nucleus and that of the host galaxy as derived from our image analysis for resolved and marginally resolved objects. Both luminosities were k-corrected and refer to rest frame R band. With our QSO sample we can explore a range of nuclear luminosity between M(R) $\sim$ -20 and M(R) $\sim$ -24 (average $<M(R)_{nuc}> =$ -22.58 $\pm$ 0.80). In this luminosity range there is not a significant correlation between the two quantities (see Fig. 11). The same result is derived if we include the compilation of low redshift quasars observed by HST (Decarli et al. 2010b) that extends to higher QSO luminosity. The only exceptions to this behaviour appears to be for few high luminosity (M(R) $\sim$ –26) quasars that are hosted in very high luminosity galaxies. A similar behaviour was also noted by McLeod & McLeod (2001) from the comparison of a collection of Seyfert galaxies and low z QSO data and interpreted as a luminosity/host-mass limit. If applied to our sample this suggests that a limit is reached when the nucleus emits (in the R band) a power corresponding to a factor 3-5 higher than the luminosity of the whole host galaxy. The same behaviour was also observed, albeit in a smaller sample, for high redshift quasars (Kotilainen et al. 2009) and confirms that an intrinsic range of accretion together with different mechanisms for low power emission may concur to destroy the correlation. Moreover it is worth to note that if the BH mass is related only with the bulge mass / luminosity then one would expect

additional disruption of the above correlation between BH and galaxy masses (see also discussion in the next section).

4.1 Host galaxy morphology

A long debated question concerning the properties of the galaxies hosting quasar is its morphology (see e.g. Böhm et al. (2013) and references therein). Do quasars inhabit both disc and bulge dominated galaxies ? This question was debated for long time since the poor spatial resolution of the observations combined with the bright nuclei hindered the clear nature of the QSO hosts. The original idea that considered radio loud QSO being hosted by ellipticals while radio quiet quasars hosted in spiral galaxies is clearly not consistent with the observations that show a more complex scenario.

In the era of HST images it was clear that at low redshift QSO are found in both types of galaxies spiral and ellipticals and also in complex morphology and interacting galaxies (Bahcall et al. 1997; Kukula et al. 2001; Ridgway et al. 2001). It was also suggested that there may be a relationship between QSO luminosity and host galaxy morphology such that all the radio-loud quasars, and all the radio-quiet quasars with nuclear luminosities M_V < -24, are massive bulge-dominated galaxies, (Floyd et al. 2004).

From the analysis of our large dataset we found that 309 out of 416 targets are well resolved (see above discussion), however, to be able to constrain the morphology of the host galaxy it is needed that the flux from the surrounding nebulosity is well detected up to large radii (faint surface brightness) where the two models ($r^{1/4}$ and exponential disk) differ significantly. In order to classify the morphology of the host galaxies we can use the values of Sersic index obtained from the best fit. In addition we also performed a fit of all objects assuming the host galaxy is a pure elliptical or a pure disk and then compared the χ^2 of the two fit. This kind of analysis can yield only a preliminary indication of the morphology of the host galaxies since in general both spheroidal and disk components may be present. In order to better characterise the host galaxies we performed a detailed visual inspection of all resolved targets using the whole information available: images, contour plots, fit of the brightness profile, ellipticity.

The morphological classification of galaxies is an important indicator of many physical processes in galaxies and the Galaxy Zoo project is a clear example Lintott et al. (2011) although it is somewhat a subjective process. For instance note that the various tools for automatic classification or the Galaxy zoo web based one can only give a rough estimate of the morphology (see e.g. Nair & Abraham (2010) for full discussion). For this reason we used the recipe of Nair & Abraham (2010) to classify our host galaxies in the same classification scheme of the Carnegie Atlas of Galaxies (Sandage & Bedke 1994) and of RC3 (de Vaucouleurs et al. (1991)). Due to the presence of the central nuclear source we restricted our T types to five main classes T=-5,-4 for all early type galaxies, T=-1 for E/S0 T=0 for S0 galaxies and T=1,2 for late type galaxies. Our classifications take into account both the visual inspection of the i band image and the luminosity profile.

From this analysis we find that the morphology of the host galaxies is rather complex with both disk and spheroidal components often present in these galaxies. Of

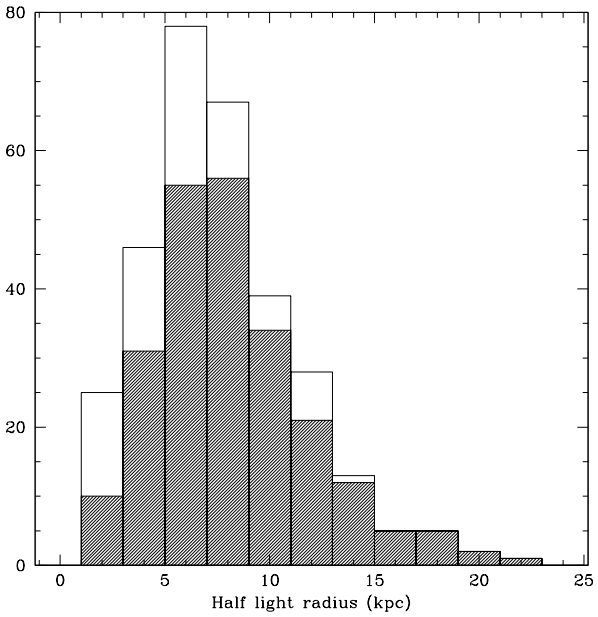

Figure 10. Distribution of half light radius of QSO host galaxies as derived from the fit with a Sersic law plus nuclear component (open histogram). In the shaded area the distribution for well resolved QSO is shown (see text). Only objects classified as resolved are included.

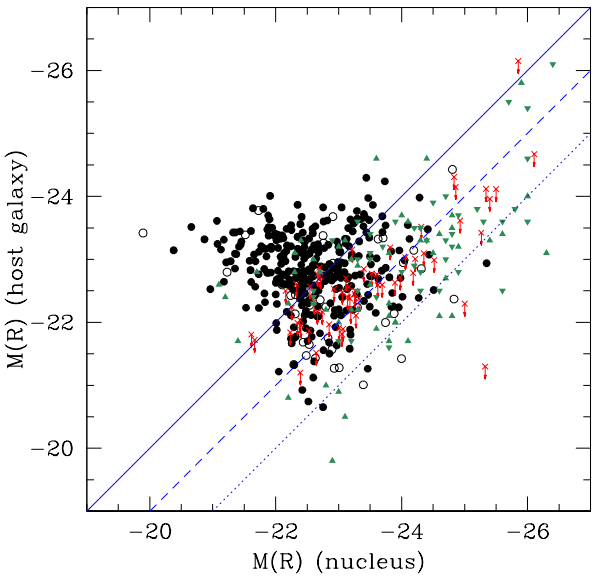

Figure 11. The comparison between the nuclear and host galaxies luminosities in the R band. Resolved quasars (filled circles), marginally resolved (open circles) and luminosity upper limits (red crosses with arrows). For comparison we include a compilation of ∼ 100 QSO host galaxies from HST observations (Decarli et al. 2010b) (filled green triangles: inverted triangles for radio loud objects) Diagonal blue lines represent the loci of fixed ratio between the nucleus and host galaxy luminosity (in the R band) at constant levels of 1 (solid line), 2.5 (dashed line), 6.25 (dotted line).

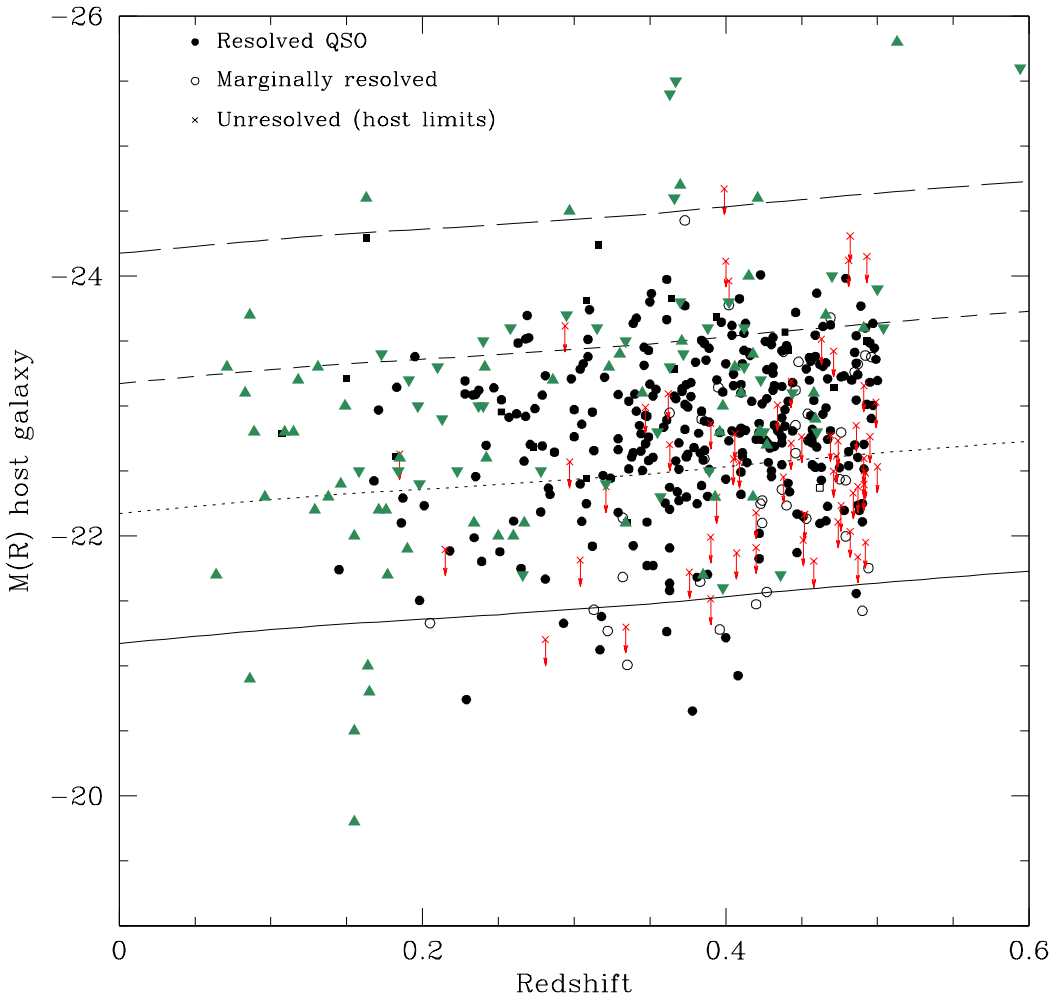

Figure 9. The absolute magnitude of QSO (RQQ circles; RLQ squares) host galaxies versus redshift. Resolved quasars (filled points), marginally resolved (open points) and luminosity lower limits (red crosses with arrows). For comparison we include a compilation of ∼ 100 QSO host galaxies from HST observations (Decarli et al. 2010b) (filled green triangles: inverted triangles for radio loud objects)

the 314 resolved targets about 113 objects (37%) are dominated by the bulge component, 129 objects (42%) have a conspicuous disk structure, 64 objects (21%) exhibit a mixed (bulge plus disk) features. For ∼100 objects (32%) a number of complex features (lens, tidal distortion, bars, close companions) are also present. Detailed analysis of these morphological structures will be presented in another paper of this series (Bettoni et al. 2014). This morphological classification of the host galaxies is summarised in Table 3.

5 BLACK HOLE MASS AND HOST GALAXY RELATIONSHIP

Massive black holes (BHs) are ubiquitously found in the centre of massive galaxies and their masses show correlations with large-scale properties of the host galaxies, namely, the stellar velocity dispersion, the luminosity, and the mass of the spheroidal component (Ferrarese 2006; Marconi & Hunt 2003; Bernardi et al 2007; Letawe, Letawe and Magain 2013). These relations have been interpreted as the outcome of a joint evolution between BHs and their host galaxies and are therefore potentially of great importance for the understanding of the processes that link nuclear activity to galaxy formation and evolution (Jahnke et al. 2009; Decarli et al.

2010b; Merloni et al. 2010; Targett, Dunlop, & McLure 2012; Cisternas et al. 2011).

Our large and homogeneous dataset allows us to investigate this relationship for low redshift quasars. For the BH mass we adopted the measurements obtained by Shen et al. (2011) who estimate the virial BH mass using the FWHM of H_β and continuum luminosity (Vestergaard & Peterson (2006)) for all the QSO in SDSS DR7 with $z < 0.7$ (Vestergaard & Peterson (2006)). All the spectra in our sample were visually inspected and 31 objects (∼7%) have been removed from the sample because of very low S/N ratio of the spectra. For three cases (i.e. objects 311, 349 and 365) we have done a new measurement of the BH mass. Since these BH masses are derived from single-epoch virial mass estimates and assume an indirect measurement of the size of the BLR from its relationship with the continuum luminosity the individual values may have large uncertainty. For our QSO sample the quoted errors of BH mass by Shen et al. (2011) taking into accounts various effects (see Shen et al. (2011) for details) range on average from 0.1 dex up to about 0.4 dex (mean error 0.17 dex) with even larger errors in few cases. Note that this uncertainty includes neither the statistical uncertainty (⩾0.3-0.4dex) from virial mass calibrations, nor the systematic uncertainties with these virial BH masses.

In Figure 12 we report the relationship between the black hole mass (M_{BH}) and the absolute magnitude of the host galaxy in the R band for all resolved quasars that have good S/N spectra (see above). The absolute magnitude M(R) of the host galaxies are in the range -22 to -24 and BH masses between 10^7 to 10^9 M_o. We search for possible evolution with the redshift of the M(R) - M(BH) relation and report in Figure 13 the comparison of the relation for different redshift intervals. From our dataset we do not find any significant evolution of the M(BH) - M(R) relation from z ∼ 0.2 to z ∼ 0.5. On average the BH masses are found systematically lower than the value expected for the host galaxy luminosity with respect to the M(R) - M(BH) relation established for local (inactive) galaxies. In addition there is a large scatter of BH masses at the same galaxy luminosity. For the galaxies of absolute magnitude -22 < M(R) < -24 the BH mass is spread over about 2 order of magnitudes. We argue that this is an indication that the BH mass is not well correlated with the total mass of the galaxy. If the BH mass is linked only with the spheroidal component then the correlation would be significantly improved. Indeed we have many quasars that are hosted in galaxies with a significant disk component therefore their bulge (or spheroid component) represent only a fraction of the total luminosity of the galaxy. In Figure 14 we show the M(BH) – M(R) (estimated bulge) relation taking into account the effects of disk/bulge components.

For each resolved quasar we have classified the morphological type of the host galaxy as described in Section 4. We have then evaluated the fraction of the bulge to total galaxy luminosity in a range between 1 to 0.3 following the above morphological classification. In Figure 14 we show the relationship between M(BH) and the estimated bulge luminosity that exhibits a significant correlation. This indicates that the BH mass is linked only with the bulges mass/luminosity and not (or only modestly) with the total mass of the galaxy. This result is also supported by the comparison of the M_{BH} host galaxy relation for 25 low redshift (z < 0.2) quasars Bentz et al. (2009a,b) for which the BH mass was derived from reverberation mapping technique and the host galaxy properties were obtained from ACS HST images. For about half of these objects the quasar host galaxy exhibits a significant disc component and a bulge to total galaxy ratio was derived Bentz et al. (2009b). For the rest of objects a pure bulge (elliptical) component was derived. It turns out that these data well overlap with our relationships for M(BH) - host galaxy (see Figure 12) and M(BH) - bulge (see Figure 14) It is worth to note that at the lowest BH masses we find QSO with relatively luminous host galaxies (see Figure 14) while those observed by Bentz et al., at similar BH masses, are significantly less luminous and lie close to the local M(R) - M(BH) relation. Since our QSO with small BH masses are well resolved it is unlikely that their host luminosity be overestimated. On the other hand note that the BH masses in Bentz et al. are measured by reverberation mapping that resolves the influence of the black hole in the time domain through spectroscopic monitoring of the continuum flux variability and the delayed response, in the broad emission-line flux. We thus argue that some bias could be in place using the virial method to derive M(BH) for low luminosity (likely lowest BH masses) QSO.

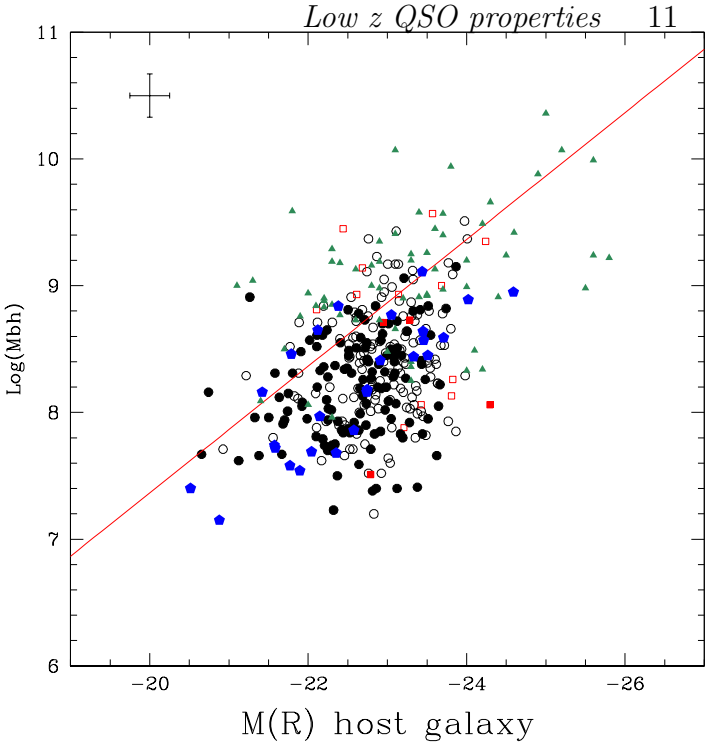

Figure 12. Absolute magnitude of QSO host galaxies versus BH mass for resolved quasars. The reference (red) line is the Bettoni et al. (2003) relation for local (inactive) galaxies for which black hole mass was measured. Open points are QSO with poor spectra and more uncertain BH masses. Red points are radio loud quasars. The mean uncertainty on BH masses is given by the error bar on the top left of the figure (see text for details). For comparison we include the compilation of QSO (green triangles) with z < 1 from Decarli et al. 2010a. The blue pentagons represent the sample of quasars observed with HST (Bentz et al. 2009a,b) and for which the BH mass was derived from reverberation mapping technique (Cales et al. 2011).

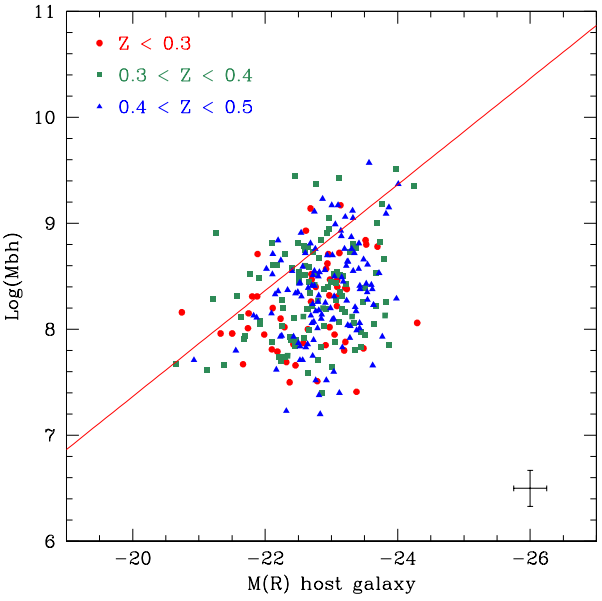

Figure 13. Absolute magnitude of QSO host galaxies versus BH mass for resolved quasars in different redshift bins. No significant difference is found among the various redshift ranges. The mean uncertainty on BH masses is given by the error bar on the bottom right of the figure (see text for details).

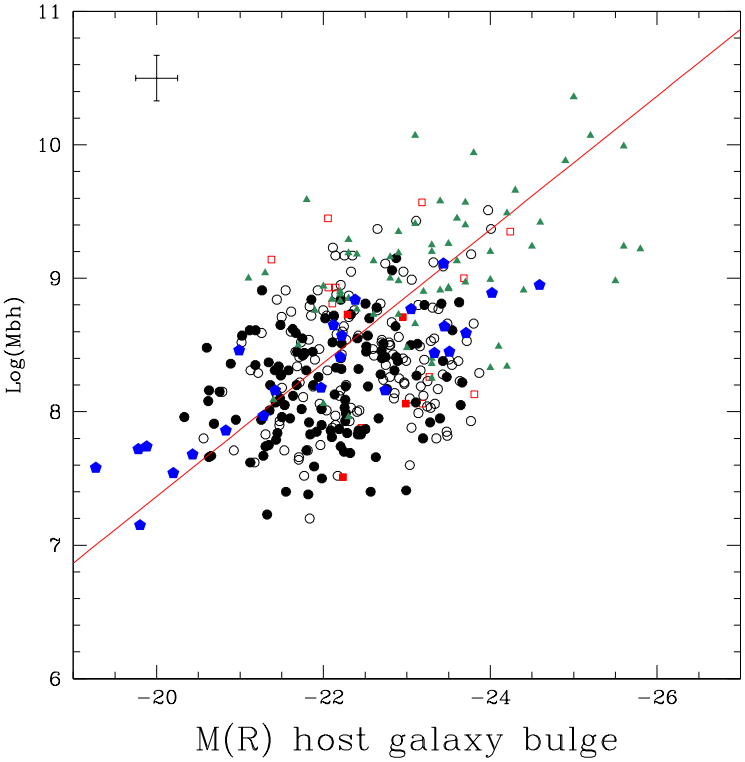

Figure 14. Same as Figure 12 but for the estimated host galaxy bulge component.

6 SUMMARY AND CONCLUSIONS

We have investigated the properties of the host galaxies from a large ($\sim$ 400 objects) and homogeneous dataset of low redshift (z < 0.5) quasars using th SDSS images in the Stripe82 region that are significantly deeper that standard SDSS data. The 2D analysis of the images allowed us to well resolve the quasar host for 3/4 of the objects in the sample, marginally resolve other 40 quasars and derive limits for the galaxy luminosity for the unresolved targets (60 objects).

The following properties of quasar hosts are derived:

(i) the luminosity of the host galaxies of low z quasars span a range from M(R) $\sim$ -21.5 to M(R) $\sim$ -24.0; the bulk of the host galaxies are located in the region corresponding to M*-1 and M*-2; there is a mild increase of the host luminosity with the redshift that is consistent with the passive evolution of the underlying stellar population

(ii) the morphology of the host galaxies turned out to be rather complex with both bulge and disc dominated galaxies; about one third of the objects in our sample show features characteristics of bulge and disc components

(iii) irrespective of the host morphology the size of the galaxies (as derived from the half light radius) ranges from compact (few kpc) objects up to extended galaxies (10-15 kpc); in the observed redshift range we do not find any significant trend of change of the galaxy size with z

(iv) the nuclear and host galaxy luminosities are not correlated suggesting that accretion rate, BH mass, and galaxy masses and morphology combine together to smear significantly the correlation between BH and host masses

(v) the BH mass of quasars estimated from the QSO continuum luminosity and the width of the broad emission lines is poorly correlated with the total luminosity/mass of the whole host galaxy; on the contrary when the fraction of bulge to disc component is considered we find a significant correlation between the BH mass and the bulge luminosity of the host.

Another important source of information to characterise the properties of low redshift QSO come from the analysis of their galaxy environments as compared with those of similar galaxies with no active nuclei. These aspects will be pursued in forthcoming papers of this series (Bettoni et al. 2014; Karhunen et al. 2013).

7 APPENDIX

In order to test the reliability of the image decomposition we have performed a number of mock simulations of quasars and then analysed them with the same method used for the Stripe82 images. To perform the simulation of the quasars we used the Advanced Exposure Time Calculator tool [1]. The parameters of the Sloan telescope and the global efficiency of the instrument were adopted from SDSS web site. We used read out noise of 9.5e, gain of 3.8 (Gunn et al. 1998), exposure time of 1 hour (subdivided in 60 exposures of 1 minute), sky brightness as average value of Kitt Peak. Statistical noise was added to the mock objects and background. The final images are background subtracted as are Stripe82 images.

Three set of simulations were performed assuming different galaxy model with Sersic index n=1, 2.5 and 4 to

[1] AETC available at http://aetc.oapd.inaf.it/

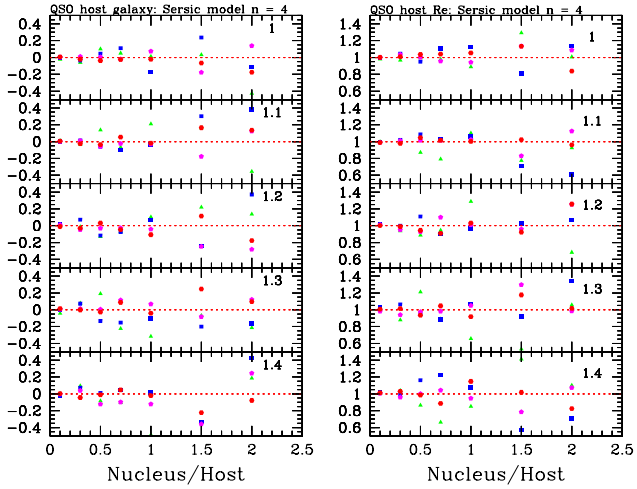

Figure 16. Mock simulation of QSO (nucleus + host galaxy with Sersic index n = 4). Left panels: Difference of the host galaxy magnitude between measured and input galaxy as a function of the nucleus/galaxy flux ratio. The panels represent simulations assuming different PSF of seeing between 1.0 and 1.4 (top right of each sub panel). The host galaxy is simulated with effective radii of 1.0 arcsec (green triangles), 1.5 arcsec (blue squares), 2.0 arcsec (magenta pentagons) and 2.5 arcsec (red hexagons). Right panel show the ratio between the measured effective radius and the true effective radius as a function of nucleus/galaxy flux ratio for the same combination of PSFs and effective radii.

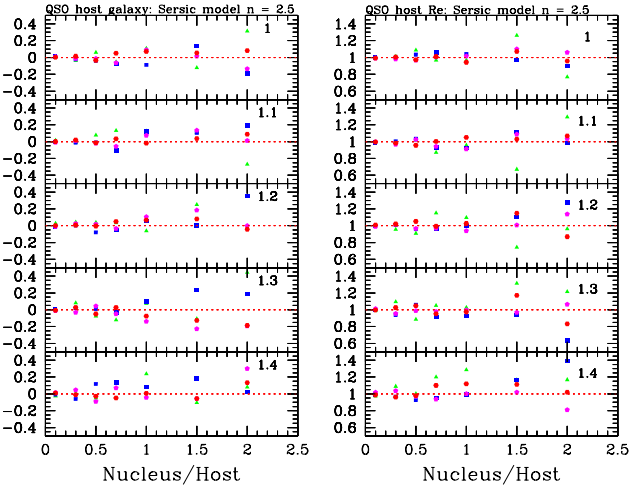

Figure 17. Same as Figure 16 but for host galaxy with Sersic index n = 2.5.

represent disk, intermediate and elliptical host galaxies , respectively. For each dataset we used a number of PSF extracted from the PSF of our images and corresponding to seeing in the range 1.0 – 1.4 arcsec (FWHM). Then we construct the QSO images as the superposition of a nucleus and a galaxy with a range of values that map the observed values. We explored a range of nucleus/host galaxy flux ratio from 0.1 to 2. Moreover for each galaxy model we assume effective radius of 1.0, 1.5, 2.0 and 2.5 arcsec (again similar to the observed parameters).

In Figure 15 we show a representative example for the three adopted host galaxy models of the mock simulations together with the fit obtained following the same procedure used for the real quasars. In Figures 16, 17, 18 we show the comparison between the measure and the true parameters of the host galaxies for the various mock simulations.

It turns out that the magnitude of the host galaxy is very well measured (< 0.1 mag) for nucleus/galaxy flux ratio smaller than 1 and seeing better than 1.2 arcsec. Also the effective radius of the host galaxy is recovered within an accuracy of 20%. For nucleus/galaxy flux ratio greater than 1 and seeing worst than 1.2 arcsec the uncertainty is larger but still adequate ($\Delta m < 0 - 3 - 0.4$) for the results presented in this work.

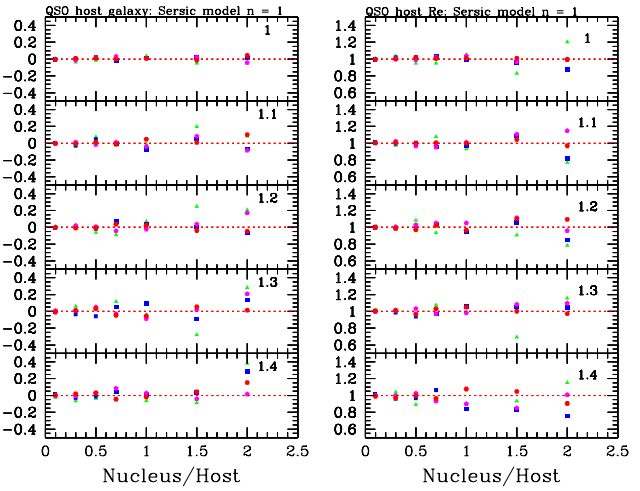

Figure 18. Same as Figure 16 but for host galaxy with Sersic index n = 1.

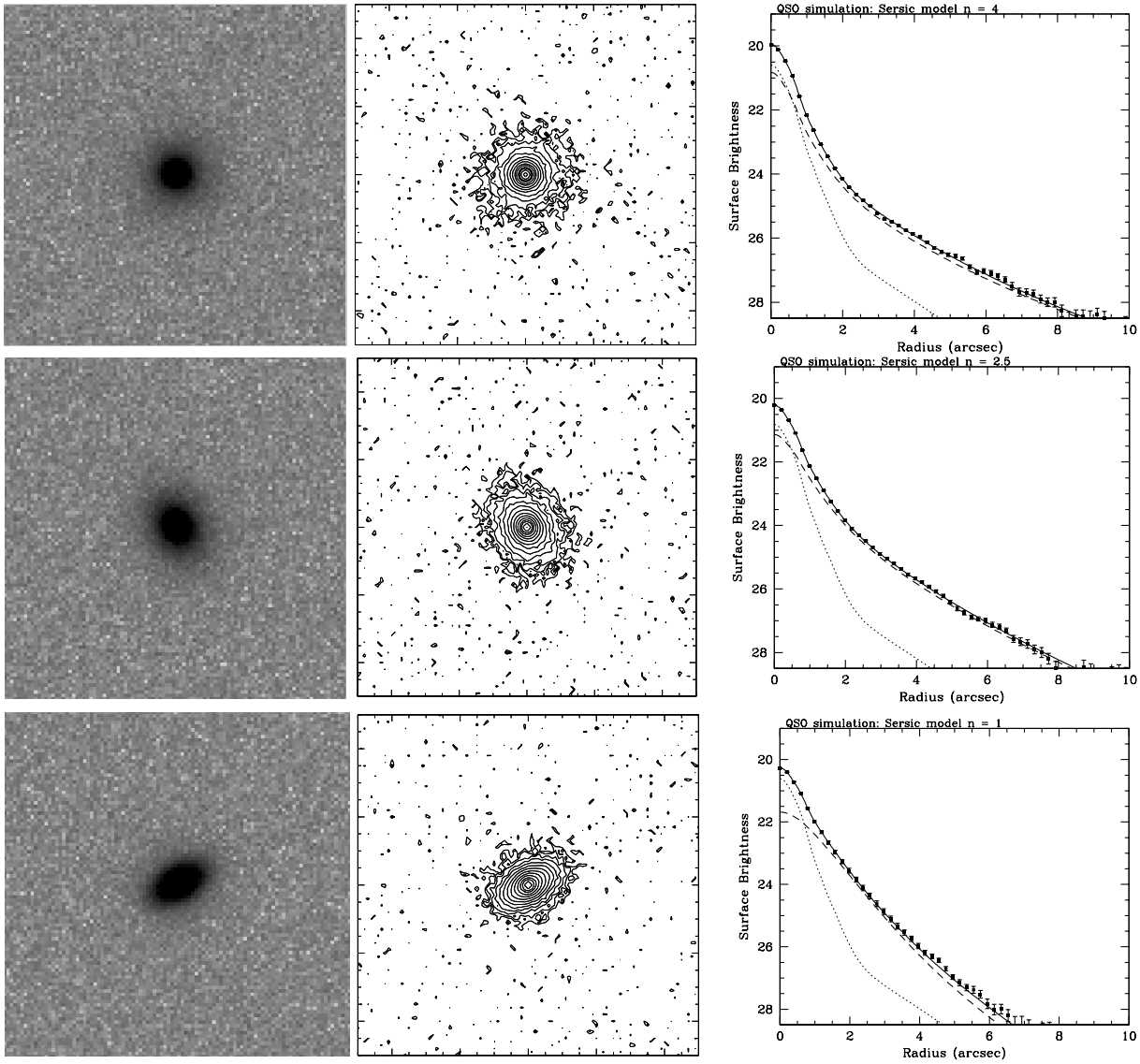
QSO simulation: Sersic model n = 4
QSO simulation: Sersic model n = 2.5
QSO simulation: Sersic model n = 1
Surface Brightness
Radius (arcsec)

Figure 15. Example of mock simulations of QSO (nucleus + host galaxy) with a Stripe82 PSF corresponding to 1.2 arcsec and nucleus/galaxy flux ratio of 0.5, and effective radius of 1.5 arcsec. Left panels show the simulated images; central panels the contour plot and the right panels the best fit of the QSO image. Top: Sersic index n = 4, ellipticity 0; Middle: Sersic index n = 2.5, ellipticity 0.3; Bottom: Sersic index n = 1, ellipticity 0.5.

Table 1. The low redshift QSO sample from SDSS82. Only first 20 items are shown. The complete table is available in electronic format.

Nr[a]	SDSS	RAJ2000	DEJ2000	z	i[b] mag	M_i mag	Nr.exp	ext(i)[c] mag	psf arcsecs
1	203657.28+000144.3	309.23868	0.02899	0.4412	19.902	-22.02	8	0.18	1.27
2	203746.78+001837.2	309.44492	0.31035	0.4503	19.58	-22.4	35	0.16	1.17
3	203905.23-005004.9	309.7718	-0.83471	0.427	19.72	-22.12	34	0.19	1.14
4	204153.51+002909.8	310.47298	0.48607	0.3969	18.554	-23.1	30	0.19	1.16
5	204340.03+002853.4	310.91681	0.48151	0.3166	18.974	-22.1	32	0.15	1.17
6	204433.61+005035.5	311.14007	0.84322	0.4854	19.599	-22.58	32	0.18	1.38
7	204527.70-003236.2	311.36543	-0.5434	0.2969	18.544	-22.37	37	0.19	1.2
8	204621.29+004427.8	311.58874	0.74106	0.4003	19.37	-22.3	40	0.23	1.28
9	204626.10+002337.7	311.60877	0.39381	0.3323	17.815	-23.38	38	0.2	1.21
10	204635.37+001351.7	311.64741	0.23103	0.4858	18.745	-23.43	38	0.22	1.21
11	204753.67+005324.0	311.97364	0.89001	0.3634	19.461	-21.96	36	0.2	1.36
12	204826.79+005737.7	312.11164	0.96048	0.4855	19.227	-22.95	34	0.2	1.35
13	204844.19-004721.5	312.18415	-0.78931	0.4655	19.814	-22.25	38	0.16	1.12
14	204910.96+001557.2	312.29569	0.2659	0.3629	19.004	-22.42	40	0.2	1.19
15	204936.47+005004.6	312.40197	0.83462	0.4751	19.952	-22.17	38	0.21	1.25
16	204956.61-001201.7	312.4859	-0.20048	0.3693	17.822	-23.64	38	0.18	1.17
17	205050.78+001159.7	312.71159	0.19992	0.3089	19.024	-21.99	37	0.22	1.09
18	205105.02-003302.7	312.77092	-0.55077	0.2999	18.957	-21.98	38	0.25	1.19
19	205212.28-002645.2	313.0512	-0.44589	0.2675	18.356	-22.3	36	0.25	1.21
20	205352.03-001601.5	313.46682	-0.2671	0.3626	18.921	-22.5	32	0.21	1.08

[a] An asterisk indicate radio loud QSO from FIRST (Becker et al. 1997, 2012)
[b] psf magnitude for filter i from SDSS-DR7
[c] Extinction from SDSS DR7 (Abazajian et al. 2009)

Table 2. The properties of QSO host galaxies. Only first 30 items are shown. The complete table is available in electronic format.

Nr	SDSS	z	nucleus mag	host mag	R_e	Chi^2_{ser}	Chi^2_{PSF}	C	T
1	203657.28+000144.3	0.4412	20.37	19.49±0.15	0.86±0.2	22.27	46.21	r	c
2	203746.78+001837.2	0.4503	19.84	>19.8	...	12.23	13.21	u	f
3	203905.23-005004.9	0.427	19.54	20.86±0.2	(0.42±0.11)	11.58	12.68	m	n
4	204153.51+002909.8	0.3969	18.97	18.55±0.15	1.7±0.17	6.64	27.06	r	c
5	204340.03+002853.4	0.3166	19.0	20.38±0.15	0.77±0.19	14.35	20.0	r	f
6	204433.61+005035.5	0.4854	19.91	19.57±0.25	(2.77±0.39)	2.53	6.15	m	c
7	204527.70-003236.2	0.2969	18.81	>18.8	...	9.44	10.78	u	f
8	204621.29+004427.8	0.4003	20.27	21.04±0.1	1.03±0.23	14.47	16.33	r	n
9	204626.10+002337.7	0.3323	17.93	19.55±0.25	(0.87±0.21)	11.64	17.23	m	c
10	204635.37+001351.7	0.4858	18.97	19.34±0.15	1.0±0.23	5.83	10.26	r	c
11	204753.67+005324.0	0.3634	19.67	19.56±0.15	1.42±0.29	7.62	19.34	r	c
12	204826.79+005737.7	0.4855	19.59	19.52±0.15	0.68±0.17	15.83	23.14	r	c
13	204844.19-004721.5	0.4655	20.05	19.34±0.1	1.39±0.28	15.48	38.89	r	n
14	204910.96+001557.2	0.3629	18.93	>19.24	...	12.52	14.24	u	c
15	204936.47+005004.6	0.4751	20.35	20.35±0.25	(0.55±0.14)	14.48	17.03	m	f
16	204956.61-001201.7	0.3693	17.57	19.45±0.15	1.27±0.27	16.02	22.92	r	c
17	205050.78+001159.7	0.3089	19.45	18.12±0.1	1.54±0.15	10.86	114.77	r	n
18	205105.02-003302.7	0.2999	19.29	18.48±0.15	2.04±0.2	3.92	36.31	r	c
19	205212.28-002645.2	0.2675	18.43	18.24±0.15	2.42±0.24	15.24	81.7	r	c
20	205352.03-001601.5	0.3626	19.1	20.32±0.15	0.61±0.16	12.54	15.39	r	f

Notes: nucleus and host magnitudes are given in the SDSS i band.
C is the class type: r=resolved object, u=unresolved ,m=marginally resolved, x=discarded object
T is the type of environment n=no feature visible, f=features visible, c=companions visible in the nearby field

Table 3. The properties of QSO host galaxies. Only first 20 items are shown. The complete table is available in electronic format.

ID	Object name	z	k-cor mag	$M_R(nuc)$ mag	$M_R(host)$ mag	R_e kpc	C	e	Morph type
1	203657.28+000144.3	0.441	0.2	-22.12	-23.04	6.88	r	0.43	e
2	203746.78+001837.2	0.45	0.19	-22.67	>-22.76	...	u	....	...
3	203905.23-005004.9	0.427	0.22	-22.89	-21.57	3.26	m	....	...
4	204153.51+002909.8	0.397	0.27	-23.29	-23.65	12.73	r	0.15	d
5	204340.03+002853.4	0.317	0.36	-22.60	-21.12	4.99	r	0.12	n
6	204433.61+005035.5	0.485	0.14	-22.76	-23.26	23.3	m	....	...
7	204527.70-003236.2	0.297	0.38	-22.54	>-22.57	...	u	....	...
8	204621.29+004427.8	0.4	0.27	-22.05	-21.22	7.75	r	0.35	n
9	204626.10+002337.7	0.332	0.34	-23.88	-22.14	5.8	m	....	...
10	204635.37+001351.7	0.486	0.14	-23.75	-23.54	8.42	r	0.19	n
11	204753.67+005324.0	0.363	0.31	-22.38	-22.37	10.06	r	0.51	d
12	204826.79+005737.7	0.486	0.14	-23.10	-23.33	5.69	r	0.3	n
13	204844.19-004721.5	0.466	0.17	-22.53	-23.33	11.44	r	0.14	n
14	204910.96+001557.2	0.363	0.31	-23.12	>-22.70	...	u	....	...
15	204936.47+005004.6	0.475	0.16	-22.31	-22.44	4.59	m	....	...
16	204956.61-001201.7	0.369	0.31	-24.51	-22.51	9.08	r	0.34	n
17	205050.78+001159.7	0.309	0.37	-22.10	-23.38	9.81	r	0.17	d
18	205105.02-003302.7	0.3	0.38	-22.15	-22.97	12.73	r	0.42	d
19	205212.28-002645.2	0.268	0.4	-22.62	-22.92	13.94	r	0.3	d
20	205352.03-001601.5	0.363	0.31	-22.97	-21.64	4.29	r	0.0	n

Note: M_R nucleus and host magnitudes are in the R band k-corrected.
R_e is effective radius in kpc; C is the e class type: r=resolved object, u=unresolved ,m=marginally resolved, x=discarded object
e is the ellipticity of the host galaxy and Morph type is the following: e=elliptical dominant, d=disk dominant, n=not classifiable.

ACKNOWLEDGMENTS

We are grateful to the anonymous referee for detailed comments that led to improve the presentation of these results. Funding for the SDSS and SDSS-II has been provided by the Alfred P. Sloan Foundation, the Participating Institutions, the National Science Foundation, the U.S. Department of Energy, the National Aeronautics and Space Administration, the Japanese Monbukagakusho, the Max Planck Society, and the Higher Education Funding Council for England. The SDSS Web Site is http://www.sdss.org/.

The SDSS is managed by the Astrophysical Research Consortium for the Participating Institutions. The Participating Institutions are the American Museum of Natural History, Astrophysical Institute Potsdam, University of Basel, University of Cambridge, Case Western Reserve University, University of Chicago, Drexel University, Fermilab, the Institute for Advanced Study, the Japan Participation Group, Johns Hopkins University, the Joint Institute for Nuclear Astrophysics, the Kavli Institute for Particle Astrophysics and Cosmology, the Korean Scientist Group, the Chinese Academy of Sciences (LAMOST), Los Alamos National Laboratory, the Max-Planck-Institute for Astronomy (MPIA), the Max-Planck-Institute for Astrophysics (MPA), New Mexico State University, Ohio State University, University of Pittsburgh, University of Portsmouth, Princeton University, the United States Naval Observatory, and the University of Washington.

REFERENCES

Abazajian, K. N., Adelman-McCarthy, J. K., Agüeros, M. A., et al. 2009, ApJ, 182, 543
Annis, J., Soares-Santos, M., Strauss, M. A., et al. 2011, arXiv:1111.6619
Bahcall J.N., Kirhakos S., Saxe D.H., Schneider D.P., 1997, ApJ, 479, 642
Becker, R. H., Helfand, D. J., White, R. L., Gregg, M. D., & Laurent-Muehleisen, S. A. 2012, VizieR Online Data Catalog, 8090, 0
Becker, R. H., Gregg, M. D., Hook, I. M., et al. 1997, ApJL, 479, L93
Bernardi M., Sheth R.K., Tundo E., Hyde J.B., 2007, ApJ,660, 267
Bettoni D., Falomo R., Fasano G., Govoni F., 2003, A&A, 399, 869
Bettoni, D. Falomo, R., Karhunen, K., Kotilainen J.K., Uslenghi, M. 2013 , in preparartion.
Bentz, M. C., Peterson, B. M., Netzer, H., Pogge, R. W., & Vestergaard, M. 2009, ApJ, 697, 160
Bentz, M. C., Peterson, B. M., Pogge, R. W., & Vestergaard, M. 2009, ApJl, 694, L166
Böhm A., et al., 2013, A&A, 549, A46
Bouwens R., Silk J., 2002, ApJ, 568, 522
Bouwens R. J., Illingworth G. D., Blakeslee J. P., Broadhurst T. J., Franx M., 2004, ApJ, 611, L1
Cales, S. L., Brotherton, M. S., Shang, Z., et al. 2011, ApJ, 741, 106
Cisternas,M., Jahnke,K., Bongiorno,A., et al., 2011, ApJ, 741, L11
Decarli R., Falomo R., Kotilainen J. K., Hyvönen T., Uslenghi M., Treves A., 2012, AdAst, 2012,
Decarli R., Falomo R., Treves A., Labita M., Kotilainen J. K., Scarpa R., 2010, MNRAS, 402, 2453
Decarli R., Falomo R., Treves A., Kotilainen J. K., Labita M., Scarpa R., 2010, MNRAS, 402, 2441
de Vaucouleurs G., de Vaucouleurs A., Corwin H. G., Jr., Buta R. J., Paturel G., Fouqué P., 1991, RC3, Springer-Verlag: New York
Dunlop J.S., McLure R.J., Kukula M.J., et al., 2003, MNRAS, 340, 1095
Falomo R., Kotilainen J.K., Pagani C., Scarpa R., Treves, A., 2004, ApJ, 604, 495
Falomo R., Treves A., Kotilainen J.K., Scarpa R., Uslenghi M., 2008, ApJ, 673, 694
Francis P.J., Hewett P.C., Foltz C.B., et al., 1991, ApJ, 373, 465
Ferrarese,L., 2006, Joint Evolution of Black Holes and Galaxies, eds. M. Colpi et al. (Taylor & Francis Group), p. 1
AJ, 135, 338
Floyd D.J.E., Kukula M.J., Dunlop J.S., et al., 2004, MNRAS, 355, 196
Floyd D.J.E., Dunlop J.S., Kukula M.J., et al., 2013, MNRAS, 429, 2
Gunn J. E., et al., 1998, AJ, 116, 3040
Letawe, Y. , Letawe, Y. and Magain, P. 2010, MNRAS, 403, 2088
Lintott, C., Schawinski, K., Bamford, S., et al. 2011, MNRAS, 410,166
Jahnke K., et al., 2009, ApJ, 706, L215
Karhunen, K. Kotilainen, Falomo, R., Bettoni,D. Usleghi, M. 2013, in preparation
Kotilainen J.K., Falomo R.,2004, A&A, 424, 107
Kotilainen J.K., Falomo R., Labita M., Treves A., & Uslenghi M., 2007, ApJ 660 1039
Kotilainen J.K., Falomo, R., Decarli, R., Treves, Uslenghi, M and Scarpa, R., ApJ 703 1663
Kotilainen J.K., Falomo, R., Bettoni, D., Karhunen, K., Uslenghi, M. 2013 arXiv:1302.1366.
Kukula M.J., Dunlop J.S., McLure R.J., et al., 2001, MNRAS, 326, 1533
Marconi A., Hunt L.K., 2003, ApJ Letters, 589, 21
Mannucci, F., Basile, F., Poggianti, B.M., et al. 2001, MNRAS, 326, 745
Matsuoka Y., Strauss M. A., Price T. N., III, DiDonato M. S., 2014, ApJ, 780, 162
Merloni,A., Bongiorno,A., Bolzonella,M. et al., 2010, ApJ 708, 137
McLeod K. K., McLeod B. A., 2001, ApJ, 546, 782
Nair, P. B., & Abraham, R. G. 2010, ApJL, 714, L260
Nakamura, O., Fukugita, M., Yasuda, N., et al. 2003, AJ, 125, 1682
Ono Y., et al., 2012, arXiv, arXiv:1212.3869
Peng,C.Y., Impey,C.D., Rix,H.-W., et al. 2006, ApJ, 649, 616
Ridgway S., Heckman T., Calzetti D., Lehnert M., 2001, ApJ, 550, 122
Sandage, A., & Bedke, J. 1994, The Carnegie Atlas of Galaxies. Volumes I, II., by Sandage, A.; Bedke, J.. Carnegie Institution of Washington Publ., No. 638
Shen, Y., Richards, G.T., Strauss, M.A., et al. 2011, ApJSS, 194, 45
Serber, W., Bahcall, N., Ménard, B., & Richards, G. 2006,

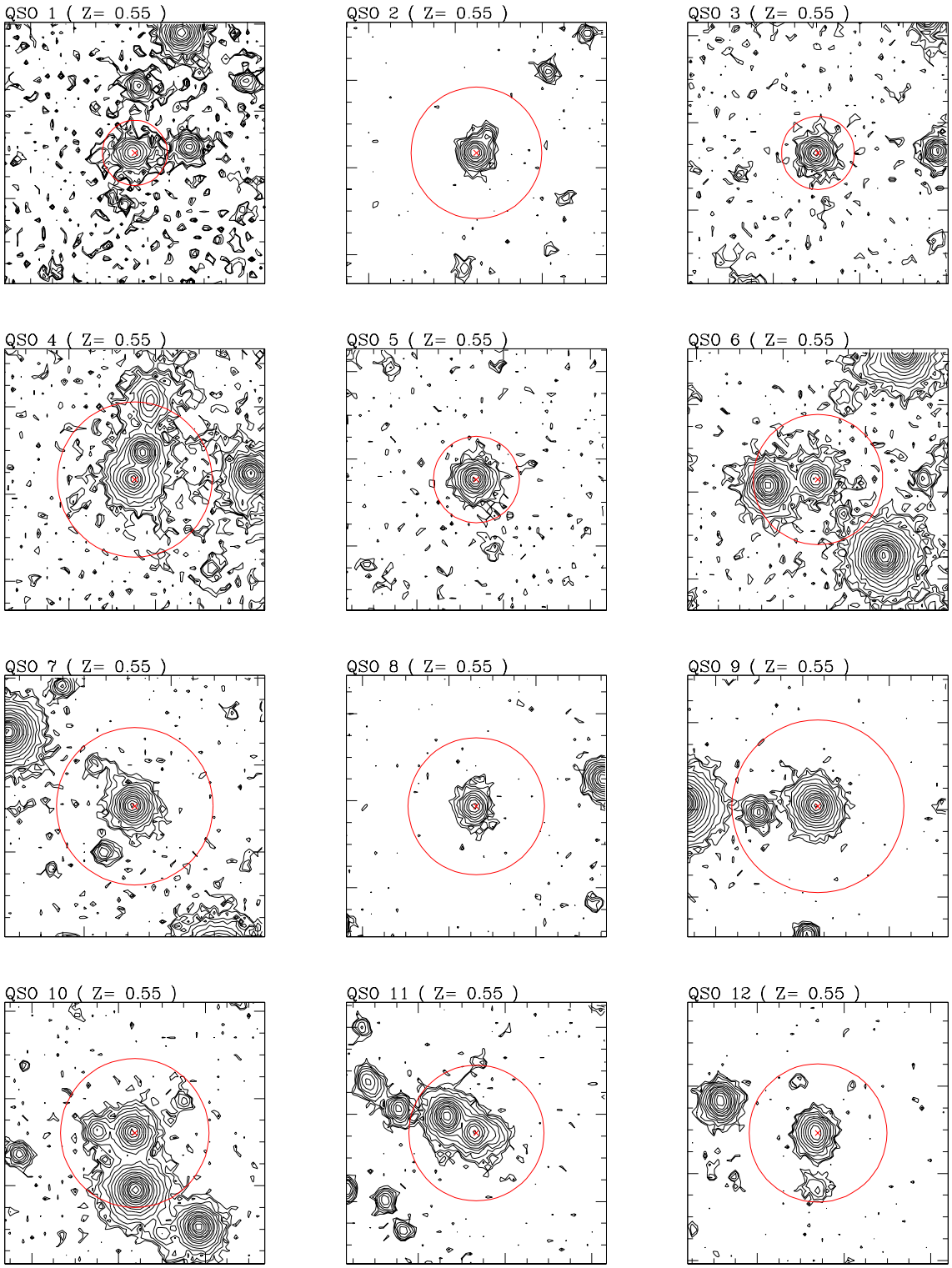

Figure 19. Contour plot of the first 12 targets (the whole figure is available as online supplementary material). The QSO is at the center of each panel and marked with a red square. The field of view in each box is 24 arcsec across. The red central circle represents the region of the fit. Masked out objects are not shown here (see example in Fig. 3)

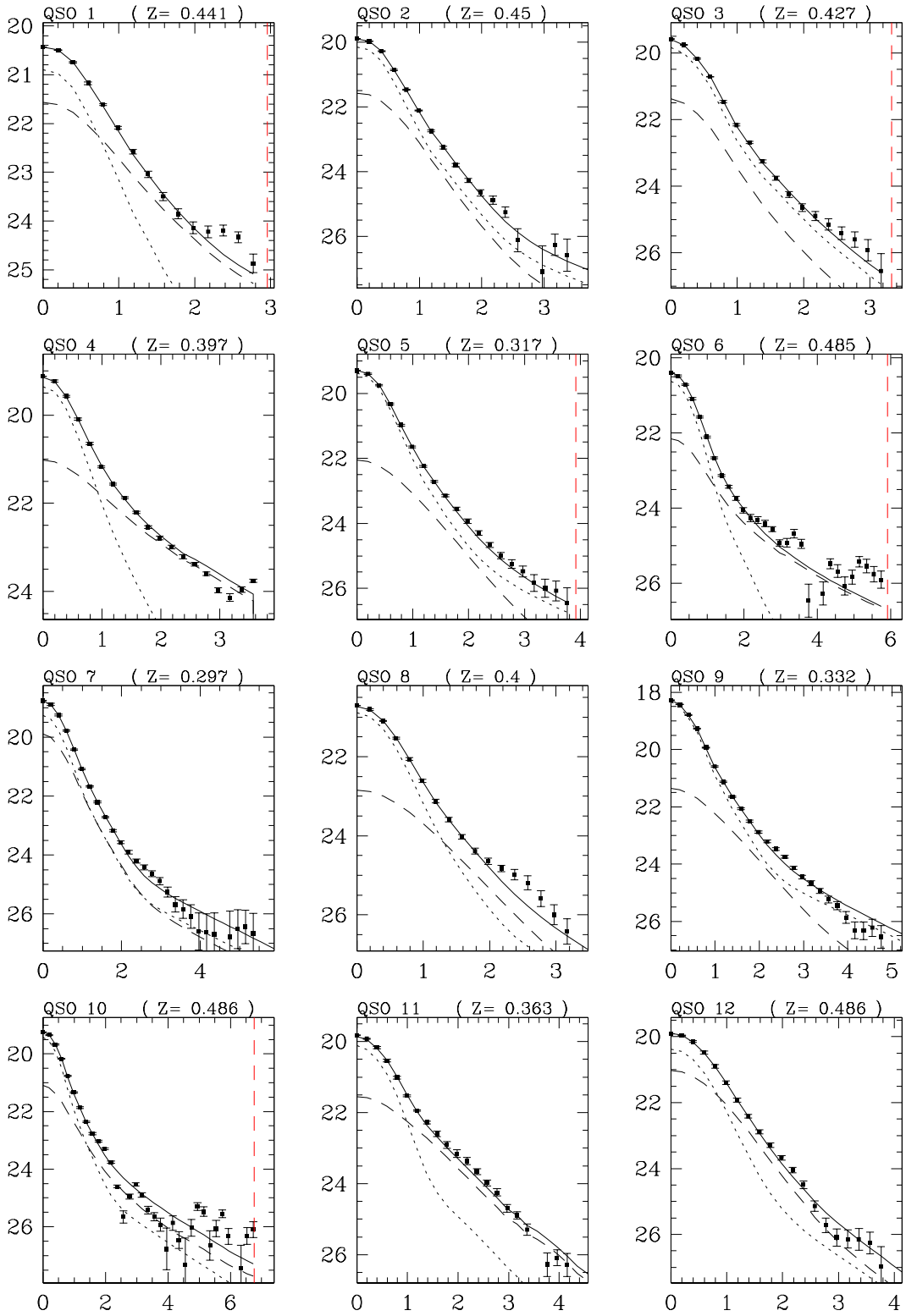

Figure 20. Fit of the first 12 targets (the whole figure is available as online supplementary material). Observed radial brightness profile (filled squares) compared with the model fit (solid line) with the two components: scaled PSF (dotted line) and galaxy model (dashed line) convolved with the proper PSF. The vertical dashed red line represents the limit of the region for the fit of the data.

ApJ, 643, 68
Schneider, D. P., Richards, G. T., Hall, P. B., et al. 2010, AJ, 139, 2360
Smith, R. J., Boyle, B. J., & Maddox, S. J. 2000, mnras, 313, 252
Strand, N. E. 2009, Ph.D. Thesis
Targett T. A., Dunlop J. S., McLure R. J., 2012, MNRAS, 420, 3621
Trujillo I., et al., 2006, ApJ, 650, 18
Uslenghi M. & Falomo, R. 2008, Proc. Erice, in press.
Vestergaard M., Peterson B. M., 2006, ApJ, 641, 689
Vestergaard M., Osmer P. S., 2009, ApJ, 699, 800
Véron-Cetty M.-P., Véron P., 2010, A&A, 518, A10
Wold M., Lacy M., Lilje P. B., Serjeant S., 2001, MNRAS, 323, 231
York, D. G. et al. 2000, AJ, 120, 1579
Zwaan M. A., van der Hulst J. M., Briggs F. H., Verheijen M. A. W., Ryan-Weber E. V., 2005, MNRAS, 364, 1467
Zakamska, N. L., Strauss, M. A., Krolik, J. H., et al. 2006, AJ, 132, 1496
Zibetti S., Ménard B., Nestor D. B., Quider A. M., Rao S. M., Turnshek D. A., 2007, ApJ, 658, 161